

We are IntechOpen, the world's leading publisher of Open Access books Built by scientists, for scientists

6,900

Open access books available

186,000

International authors and editors

200M

Downloads

Our authors are among the

154

Countries delivered to

TOP 1%

most cited scientists

12.2%

Contributors from top 500 universities



WEB OF SCIENCE™

Selection of our books indexed in the Book Citation Index
in Web of Science™ Core Collection (BKCI)

Interested in publishing with us?
Contact book.department@intechopen.com

Numbers displayed above are based on latest data collected.
For more information visit www.intechopen.com



Fabrication and Characterization of Organic–Inorganic Hybrid Perovskite Devices with External Doping

Kongchao Shen, Hao Liang Sun, Gengwu Ji,
Yingguo Yang, Zheng Jiang and Fei Song

Additional information is available at the end of the chapter

<http://dx.doi.org/10.5772/63771>

Abstract

Owing to its excellent light harvesting, high-charge carrier mobility, and long electron- and hole-transport lengths, organic–inorganic lead halide perovskite solar cells have attracted enormous attention recently under the urgent demands of green energy with environmental friendliness. Although various photovoltaic architectures based on alkylammonium lead halides have been fabricated and have achieved impressive power conversion efficiencies (PCEs), there are still several issues that need to be further addressed and solved properly, for example, the requirement of facile fabrication procedure, the chemical stability of perovskite films, and the environmental friendliness. Herein, we review the recent experimental progress on the external doping of hybrid perovskite devices by organics and metals, which demonstrate the tuning of optical absorption gap and the enhancement of both devices' stability and performance. Doping at varying layers in the perovskite films was discovered to contribute differently to the improvement of the hybrid organic–inorganic electronics. In the end, prospective was also made on the development of hybrid organic–inorganic devices.

Keywords: hybrid organic electronics, perovskite solar cells, external doping, device performance, stability

1. Introduction

Depletion of fossil fuels and the shortage of energy has become one of the most serious problems nowadays, which strongly restricts the sustainable development in our soci-

ety. To achieve a sustainable society, we need methods of converting energy from other resources, such as wind and sunlight. Among the proposed approaches, photoelectrochemical devices offer the promise of solar fuel production through artificial photosynthesis and led to considerable development in numerous areas related to photovoltaic cells and electronics. Thin-film solar cells, such as dye-sensitized solar cells, organic photovoltaics, and colloidal nanocrystal solar cells, can be assembled with low-cost materials and manufactured with cost-effective methods and are considered very promising renewable energy technologies. Especially, hybrid organic–inorganic perovskites based on the metal halides have emerged as one class of promising light-harvesting materials because of their exceptional properties such as direct band gaps, large absorption coefficients, and high carrier mobility. Meanwhile, the organic–inorganic perovskite solar cell also have many other advantages compared to the conventional solar cells, such as easy solution process, low processing cost, extremely high power conversion efficiency which reached over 20% recently. All these merits have granted perovskite a promising candidate for the next-generation solar cells.

Although great success in the use perovskite solar cells has been witnessed over the past few years, there are still several bottlenecks which limit significantly the wide deployment of its outdoor application: for example, the poor stability of the perovskite film and the charge transport layers, dangers and health risks arising from toxic and harmful element due to the usage of lead and other heavy metal atoms. Based on these urgent demands and concerns, the improvement of perovskite electronics has been explored and demonstrated. Interestingly, doping of perovskite electronics seems to be an efficient way to enhance both the stability and performance of perovskite electronics, which is at moment classified into several approaches: doping into the electron transport layer, doping into the perovskite films, and doping into the hole transport layer. In this chapter, we review the progress of in situ fabrication and characterization of organic–inorganic hybrid electronics by external doping and propose some of them.

2. Structure and performance of perovskite electronics

Since 2009, Kojima and his coworkers used $\text{CH}_3\text{NH}_3\text{PbBr}_3$ and $\text{CH}_3\text{NH}_3\text{PbI}_3$ as sensitizers in solar cell; great progress has been made for such kind of solar cells not only due to the fact that the power conversion efficiency (PCE) is increased from 3.8 to 20.8% [1,2], but also that it has high absorption characteristics, appropriate direct band gaps, high carrier mobility, long charge carrier diffusion length, low cost, and easy fabrication processes [3]. All these excellent performances are mostly originated from the **organic–inorganic perovskite film**. The formula of perovskite is usually written as ABX_3 , where A is an organic cation, e.g., CH_3NH_3^+ , B is a metal cation, e.g., Pb^{2+} , and X is a halide anion, as shown in **Figure 1a**.

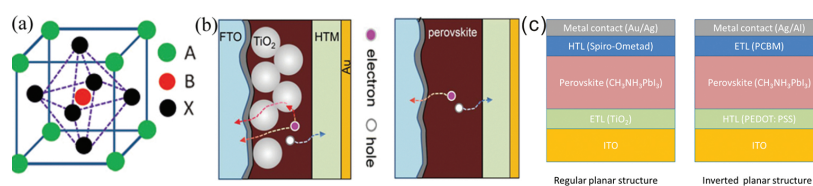


Figure 1. (a) Illustration of the organic–inorganic perovskite structure; (b) mesoporous and planar structure of hybrid perovskite devices; (c) the comparison between regular and inverted structure of hybrid perovskite device.

The sandwich-like structures of the organic–inorganic hybrid perovskite devices are shown in **Figure 1b**. Mesoporous structure and planar structure (**Figure 1b**) are the so-called positive structure, while the inverted structure is presented in **Figure 1c** with the electron transport layer (ETL) and the hole transport layer (HTL) upside down as compared to the regular perovskite structure device. As discovered, the inverted structure can reduce J-V hysteresis and is more stable due to the hydrophobic PCBM ([6,6]-phenyl-C61-butyric acid methyl ester) and its easy fabrication. With the thin perovskite layer placed between the HTL and the ETL under illumination, voltage/current is formed by generating and directionally moving the excitons (holes and electrons) after overcoming the energy barrier of the band gap. Electron–hole pairs are generated almost instantaneously after photo excitation and dissociated in the time scale of several ps, followed by the formation of high mobile charges in the neat perovskite [4]. After the generation and separation of excitons, the holes and electrons diffuse to the opposite site of the sensitizer to reach electrodes forming electrical current; however, not all of the holes and electrons can get to the electrode and contribute to the power generation, since some of them will be captured by the defects or recombined with other electrons/holes on the way to electrodes. The routes of carrier transmission are illustrated in **Figure 2**.

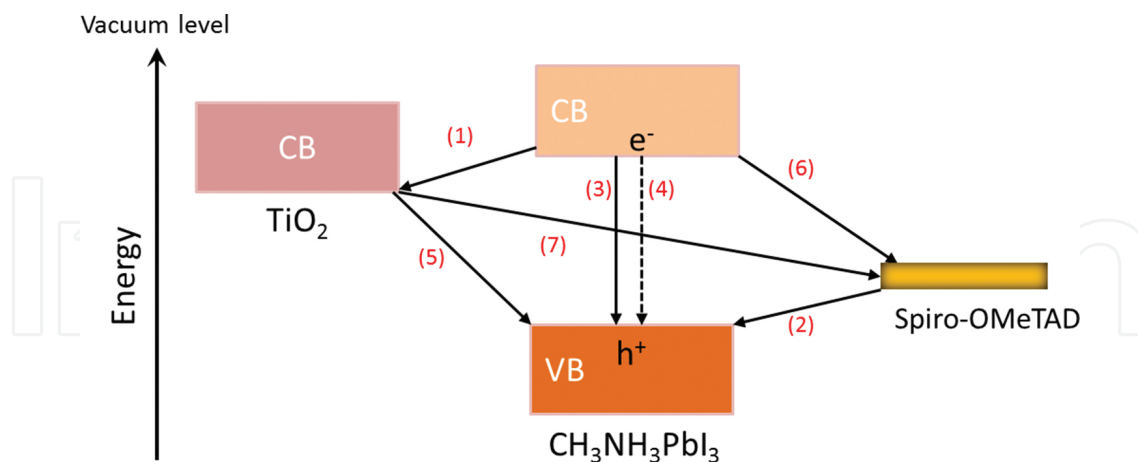


Figure 2. Schematic diagram of energy levels and electron transfer processes in an HTM/perovskite/TiO₂ cell. (1) Electron injection; (2) hole injection; (3) radiative exciton recombination; (4) non-radiative exciton recombination; (5) back electron transfer at the TiO₂ surface; (6) back charge transfer at the HTM surface; (7) charge recombination at the TiO₂/HTM interface.

With various cations/ions in the perovskite structure, there are different lattice parameters. However, it is not always suitable to have random combinations of cation A, B, and anion X.

The crystallographic stability and probable structure can be evaluated by considering the Goldschmidt's tolerance factor t and the octahedral factor μ [5], $t = (r_A + r_X)/[\sqrt{2}*(r_B + r_X)]$, where r_A , r_B , and r_X are the effective ionic radii for the ions in the A, B, and X sites, respectively. This allows us to estimate the degree of distortion of perovskite crystal structure compared to the ideal case where $t = 1$. The octahedral factor (μ) is an additional consideration for perovskite formability, where $\mu = r_B/r_X$. It has been generally accepted that the perovskite was stabilized for a tolerance factor ranging between 0.813 and 1.107 and an octahedral factor ranging from 0.442 and 0.895 [6]. It has been found that hybrid organic–inorganic devices usually degrade easily and quickly on exposure to the moisture or ultraviolet radiation [7]. Meanwhile, structural phase transformations of conventional hybrid perovskite films at different temperature ranges are also listed in **Table 1**. Still, there have been reports on the formation of single crystals when the conditions of saturation, nucleation, and growth are well controlled [8–11].

PSC	Phase	Temperature (K)	Structure	Space group	Lattice parameter (Å)
MAPbI ₃	α	400	Tetragonal	<i>P4mm</i>	a=6.3115 b=6.3115 c=6.3161
	β	293	Tetragonal	<i>I4cm</i>	a=8.849 b=8.849 c=12.642
	γ	162–172	Orthorhombic	<i>Pna2₁</i>	a=5.673 b=5.628 c=11.182
MAPbCl ₃	α	>178.8	Cubic	<i>Pm3m</i>	a=5.675
	β	172.9–178.9	Tetragonal	<i>P4/mmm</i>	a=5.655 c=5.630
	γ	<172.9	Orthorhombic	<i>P222₁</i>	a=5.673 b=5.628 c=11.182
MAPbBr ₃	α	>236.9	Cubic	<i>Pm3m</i>	a=5.901
	β	155.1–236.9	Tetragonal	<i>I4/mcm</i>	a=8.322 c=11.833
	γ	149.5–155.1	Tetragonal	<i>P4/mmm</i>	a=5.8942 c=5.8612
	δ	<144.5	Orthorhombic	<i>Pna2₁</i>	a=7.979 b=8.580 c=11.849
MASnI ₃	α	293.00	Tetragonal	<i>P4mm</i>	a=6.2302 b=6.2302 c=6.2316
	β	200	Tetragonal	<i>I4cm</i>	a=8.7577 b=8.7577 c=12.429
FAPbI ₃	α	293	Trigonal	<i>P3m1</i>	a=8.9817 b=8.9817 c=11.006
	β	150	Trigonal	<i>P3</i>	a=17.791 b=17.791 c=10.091

Table 1. Structural phase transformations for common hybrid perovskites. The table was taken from [5] with permission.

The thickness of this sensitized layer is usually limited to be around several hundred nanometers concerning the fact that holes and electrons will be recombined quickly if the film thickness is thicker than the diffusion length of charge carriers. Therefore, we simply consider the diffusion length of excitations which depend not only on the amount but also on the concentration of precursors [12–14]. As known, the nature of ambipolar of the perovskite material leads to the transport of both electrons and holes [15]. For example, the trioxide

absorber $\text{CH}_3\text{NH}_3\text{PbI}_3$ has the electron–hole diffusion length of several hundred nanometers and a relatively long life time [16].

Even though hybrid perovskite films are expected to have such appealing properties, only the elaborate design of every counterpart of the whole device can make the performance of hybrid perovskite devices as great as possible. For example, the band level alignment of different layers and materials in devices should be considered carefully. As summarized from literatures, the energy bands of ETL must satisfy the following conditions [17]: (1) Its conduction band (CB) must lie under the CB of the active perovskite layer to extract electrons which reach the interfaces afterward. (2) Its valence band (VB) must lie much under the VB of the perovskite to reject the holes. (3) The electron affinity of the ETL must be greater than that of the perovskite. (4) The VB of ETL should have large difference compared to the VB of perovskite in order to reject holes, so the ETL usually has wide band gap. (5) The electron mobility in ETL must be sufficiently high. Similar requirements can also be deduced for HTL. The values of VB and CB of some commonly used materials are listed in **Figure 3**.

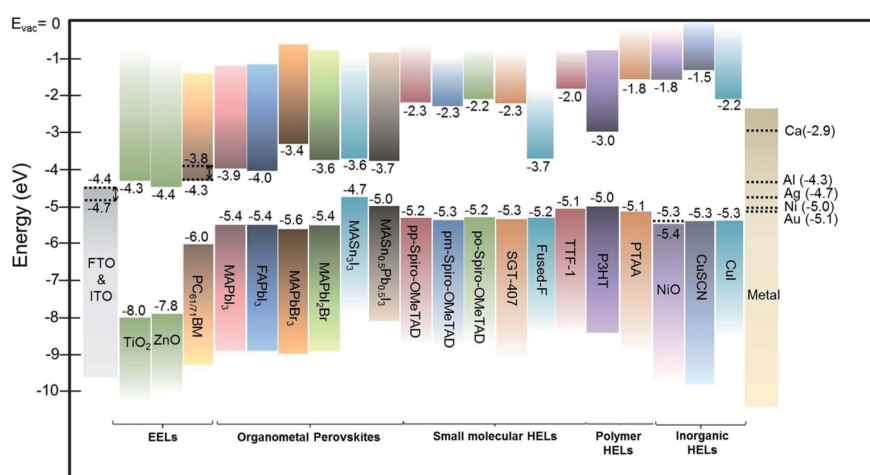


Figure 3. The VB and CB of various perovskite films. The figure was taken from [17] with permission.

The exciton property, electrical property, and the energy band of various ETL/HTL materials have been discussed so far. Moreover, optical properties will also be illustrated in this section. The mostly used technique to explore the optical property is ultraviolet-visible (UV) and photoluminescence (PL) spectroscopy. Different UV/PL spectra are shown in **Figure 4a** and **b** [18, 19]. The absorption edges of perovskite films in **Figure 4** clearly indicate that hybrid perovskite devices have high absorption factor at visible and near-infrared range, which just fit well to the solar spectrum. **Figure 5** shows the complementarities between the Si-based solar cell and the hybrid perovskite device as they have opposite external quantum efficiency (EQE). Furthermore, the internal quantum efficiency (IQE) has been reported to reach 100% through optimizing the perovskite device [20], which inspires the researchers that tandem solar cells based on perovskite, and Si is very interesting if the fabrication technology can be improved to use the sunlight more effectively.

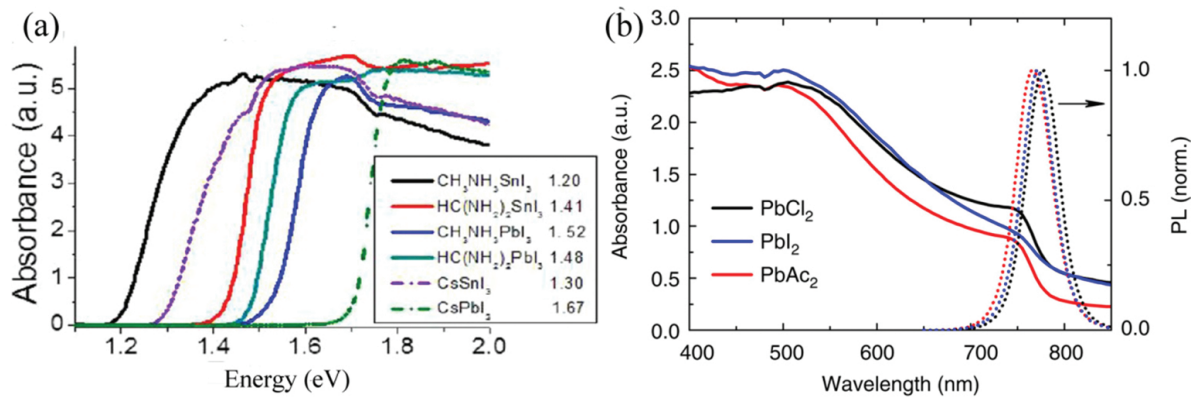


Figure 4. (a) Various sites A and B have different band gaps. The value of the band gap is given next to each compound. Figure was taken from [18] with permission; (b) UV-vis absorption spectra for perovskite films derived from different lead sources. The right axis shows the PL spectra of the perovskites prepared on glass, with photoexcitation at 507 nm. The figures are taken from [19] with permission.

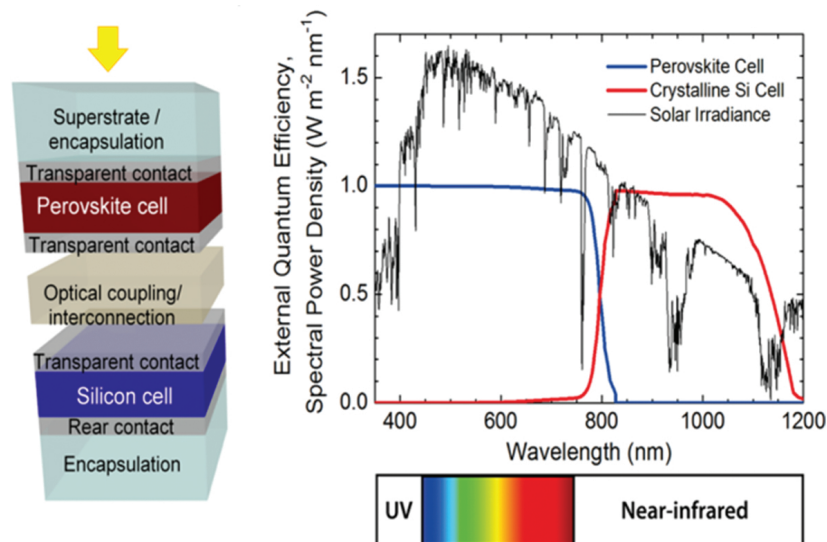


Figure 5. The complementation of EQE in Si and perovskite tandem solar cell. The image was taken from pvlab.epfl.ch/page-124775-en.html with permission.

3. Doping into different layers and the influence on devices

3.1. Doping into the electron transport layer

As discovered, the boundaries and defects existing in ETL generally result in the recombination of electrons and holes associated with pinhole/cracks between ETL and substrate and will therefore lead into the decline of PCE and stability. Consequently, proposed materials for ETL should own high electron affinity, excellent surface morphology, and effective hole-blocking properties. From this point of view, visible improvement should be realized by properly

doping the ETL for the electron transport property, the hole blocking ability, since external doping usually rearranges the band alignment due to the pinning of Fermi level, which may influence the electron transport property, hole blocking ability, for example, in the manner of removing deep electronic traps and sub-band states, enhance the carrier's life time and the film's conductivity by several orders of magnitude. Meanwhile, the doping into ETL can also enhance the film morphology by removing defects or filling the gap in between islands in the film. Nevertheless, the band gap of ETL itself is also modified by doping due to the change of band structures. In the following, mostly used electron transport materials are described in detail.

3.1.1. TiO_2

Rutile TiO_2 nanostructures on fluorine-doped tin oxide (FTO) substrates are interesting building blocks for solar cells (as shown in **Figure 7a**). Rutile structure and FTO substrate are always adopted together for the electron transport material, since FTO can be annealed up to 450°C when rutile TiO_2 is formed. The properties of large band gap, suitable band edge for charge injection and extraction, long lifetime of excited charge carriers, exceptional resistance to photo corrosion, non-toxicity, and low cost have made TiO_2 a popular material for solar energy applications. In spite of this, pure TiO_2 is not ideal for ETL which need to be doped to achieve n-type characters for higher electron extraction.

The scale of the pure TiO_2 nanoparticles which results in the highest PCE in organic–inorganic devices is about 50 nm [21]. The crafts for the fabrication of compact TiO_2 layer (spin coating, spray pyrolysis, sol-gel methods, magnetron sputtering) have developed rapidly, and one effective way is to decorate TiO_2 in order to improve the device's performance. For example, Mg-doped TiO_2 can increase the open-circuit voltages (V_{OC}) originated from elevating CB by a microwave hydrothermal reaction [22]. Yttrium-doped TiO_2 (Y- TiO_2) was used as the ETL to enhance electron extraction and transport [23]. Zr/Pyridine-doped TiO_2 could reduce the hysteresis and improve the performance of organic perovskite device by increasing the carrier's lifetime [24]. Nb-doped TiO_2 reduced selectively the contact resistance and increased the charge recombination resistance, as revealed by the impedance spectroscopy measurements [25]. A low level of Al doping into TiO_2 , by adding the aluminum isopropoxide precursor into Ti isopropoxide solution, can reduce non-stoichiometric oxygen-induced defects in TiO_2 layer. As discovered, the substitution/doping removes deep electronic traps and sub-band states, enhances the conductivity by several orders of magnitude, and improves the stability of corresponding devices. In all, metal doping of TiO_2 seems to be the main method, while other approaches of doping also exist, for example, TiO_2 mixed with graphene, which promises the low cost as the compact ETL synthesized by solution-based deposition procedure [26]. Another doping-like method is inserting ultrathin graphene quantum dots (GQDs) between TiO_2 and perovskite layer, which could reduce the electron extraction time from 300 to 100 ps [27]. Nevertheless, we should bear in mind that most of these doping methods have been utilized in dye-sensitized solar cells. Traps appear after doping in TiO_2 , and new energy levels are formed. As can be seen in **Figure 6**, the doping concentration determines the operation mechanism of electron and affects the V_{OC} and short-circuit current (J_{SC}) [28].

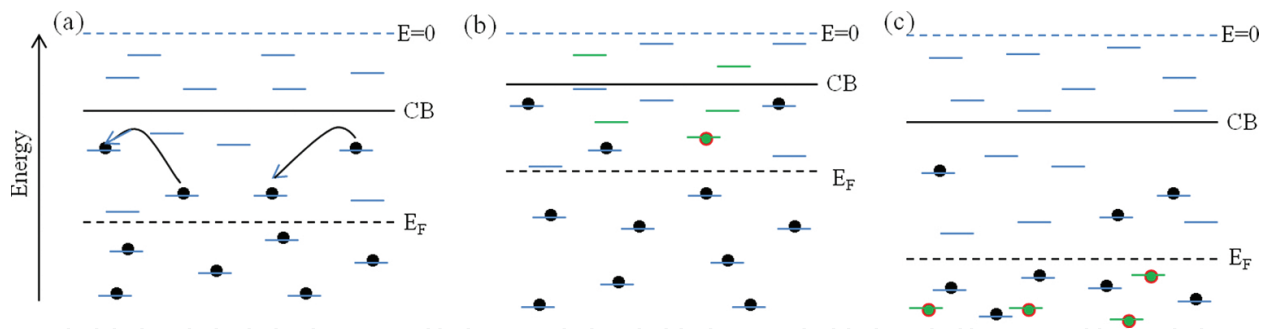


Figure 6. Illustration of the doping effect on the CB and E_F in TiO_2 . E_F is the Fermi level, and the doping induced states are also displayed in green. (a) In pristine TiO_2 , electrons are transported by “hopping” from shallow trap to shallow trap until getting to the electrode. Therefore, the electron transport rate and J_{SC} will be affected by the density of shallow trap. Deep traps can permanently trap electrons and act as recombination sites, affecting V_{OC} . Another important factor determining V_{OC} is E_F , as V_{OC} is defined as the difference between E_F of TiO_2 and the HTM. (b) The elimination of the deep trap density, resulting in an upward shift of E_F and thus an increase of V_{OC} . Because the CB is shifted toward the CB of the absorber, the driving force for electron injection is lowered, in combination with a decreased trap density and the related electron transport, lowering J_{SC} . (c) In the case of formation of deep traps by doping, the CB and E_F are shifted downward. Together with the enhanced recombination through the deep trap states V_{OC} decreases. Due to the larger offset between the CB and the absorber CB, electron injection is improved and the higher trap density causes an increase in electron transport, resulting in an enhanced J_{SC} . Ideally, the dopant eliminates deep traps while introducing new states close to CB, enhancing both V_{OC} and J_{SC} through decreased recombination and increased electron transport.

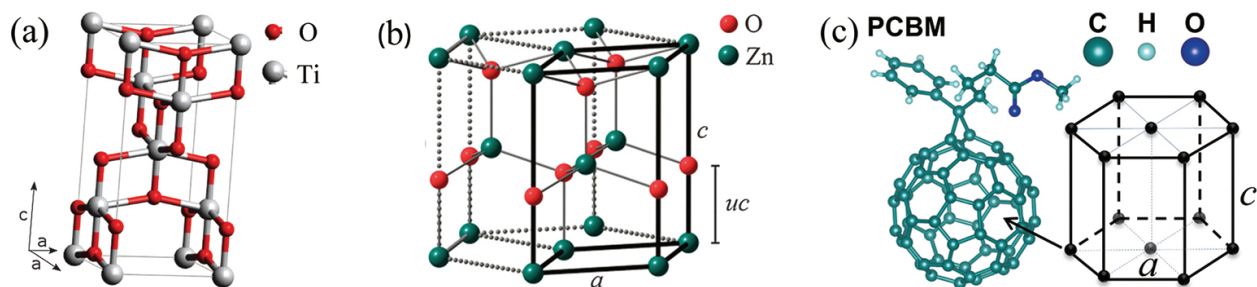


Figure 7. (a) The unit cell of TiO_2 ; oxygen atoms form a distorted octahedron with a titanium atom at the center; (b) the ZnO unit cell; (c) the molecular drawing of the PCBM with the unit cell labeled.

On the contrary, the size of the particles used as mesoporous TiO_2 is very small (around 15 nm) and can be easily controlled by tuning the concentration, pH of the reactants, and the annealing temperature. As also discovered, reduced graphene oxide/mesoporous TiO_2 nanocomposite as scaffold material could improve the electron collection efficiency, enhance the V_{OC} and J_{SC} , and reduce the interface resistance [29]. Doping into the mesoporous TiO_2 has been tried by self-assembling one monolayer of fullerene (C_{60}) to get a functionalized mesoporous titania for good electron extraction [30].

3.1.2. ZnO

Compared to TiO_2 , ZnO (**Figure 7b**) owing to high electron collection as ETL is more environment friendly as it does not need to be sintered as high as to 450°C to become rutile crystal and

grows very fast by solution process [31]. Furthermore, less chance of recombination of carriers would occur in ZnO because its conductivity is several orders of magnitude higher than that of TiO₂ [32–34]. As known, ZnO is an important II–VI semiconductor with a direct band gap of 3.4 eV and an exciton binding energy of 60 meV at room temperature. Moreover, ZnO has excellent optical properties such as a high infrared reflectivity and transparency in the visible spectrum. In addition, it is abundant in nature and inexpensive [35]. However, ZnO accelerates the degradation of perovskite layer into PbI₂ when it is thermally annealed [36]. Similar to TiO₂, ZnO also suffers from photo corrosion which reduces the performance and stability [37].

As reported, Al-doped ZnO lifted the PCE from 10.8 to 12.0% by optimizing the thickness of ETL and smoothing the interface [38]. Though fewer reports have been found for the doping of ZnO till date, it is proved gradually to be an excellent candidate with external doping to replace TiO₂ and to solve the problems existing in TiO₂. In a word, metal atoms are always chosen to be the doping materials in the doping of either TiO₂ or ZnO.

3.1.3. PCBM

PCBM (**Figure 7c**) is one of the fullerene derivatives. Its excellent properties of high electron affinity and transmission make it extremely popular in organic solar cells. PCBM is widely used in inverted perovskite structure accompanied with indium tin oxide (ITO) substrate.

PCBM doped with 1,3-dimethyl-2-phenyl-2,3-dihydro-1H-benzoimidazole (DMBI) results in n-doped ETL which significantly increases the J_{sc} [39], while oleamide-doped PCBM improves the property of electron transport [40]. It has also been reported that PCBM doped with graphdiyne [41], and the inverted hybrid perovskite structure spun with PCBM/C₆₀ could reduce the traps effectively which passivates the charge trap states and eliminates the notorious photocurrent hysteresis [42, 43]. Moreover, PCBM doped with PFNOX and polystyrene (PS) was found to enhance J_{sc} , while negligible hysteresis was discovered due to PFNOX which reduced the electron recombination [44]. The advantages of PCBM compared with metal-oxide ETL are that it can be used in soft hybrid perovskite devices with soluble process at the cost of low power consumption.

3.2. Doping into the perovskite layer

3.2.1. Doping at site A

The cation at site A has no direct contribution to the properties of electron injection or transport. The B–X octahedra and A are relatively independent owing to the fact that there is almost no overlap between the electron clouds of A and B–X due to the large unit cell [45]. However, the radius of ion A affects the symmetry of the perovskite structure which in turn affects the electron's properties [46–48]. As summarized from literatures, site A is always occupied by Cs, Rb, methylammonium (MA), formamidinium (FA), or ethylammonium (EA). The first study about mixed cations (MA)_x(FA)_{1-x}PbI₃ claimed that the PCE reaches up to 14.9% due to the changing band gap which facilitates the photon absorption much more effectively [49]. Afterward, (MA)_x(FA)_{1-x}PbI₃-based hybrid devices have been fabricated with rather high PCE [46,

48, 50]. **Figure 8a** and **b** shows the difference in emission spectrum and the change of light harvesting due to different ratios of FAI and MAI in hybrid perovskite solar cells. Similar discoveries were also reported by our group when doping MA with small amount of CH_3SH organics, while the PCE increased from 6.9 to 9.4% [51], as presented in **Figure 8c**. When site A is doped by Cs with optimized doping concentration and film thickness, the PCE reaches over 10%, and the film morphology was found to be more compact and uniform [52]. For example, PCE over 17% was reported for the $\text{Cs}_{0.2}\text{FA}_{0.8}\text{PbI}_{2.84}\text{Br}_{0.16}$ hybrid device as well as the excellent stability in ambient air compared to FAPbI_3 , which was attributed to uniform coating on TiO_2 and no separation in chemical phases [53]. Methylammonium(MA) iodide and 5-ammoniumvaleric acid (5-AVA) iodide hybrid perovskite device was also found to have high stability of perovskite structure and performance [54], which can be attributed to the lower defect concentration and better pore filling as well as complete contact with the mesoporous scaffold, as illustrated in **Figure 8d**.

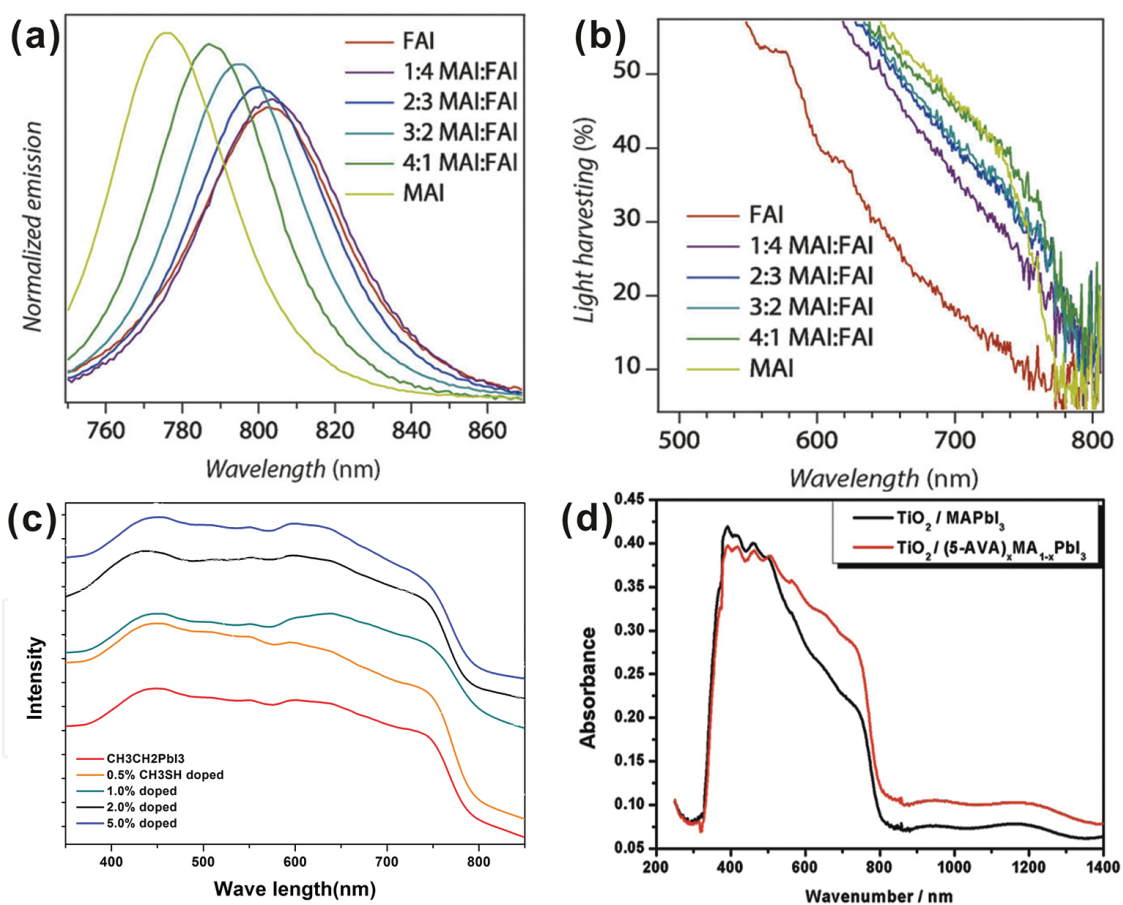


Figure 8. (a) Normalized emission of $(\text{CH}_3\text{NH}_3)_x(\text{HNCHNH}_3)_{1-x}\text{PbI}_3$ ($x = 0, 0.2, 0.4, 0.6, 0.8, 1$). The emission is shifted and broadened as a function of x . (b) Light-harvesting spectra of $(\text{CH}_3\text{NH}_3)_x(\text{HNCHNH}_3)_{1-x}\text{PbI}_3$ films with different x . As the concentration of formamidinium was increased, the absorbance of the film decreased, while no change in the band gap was discernable. (c) UV absorption spectra of $(\text{CH}_3\text{SH}_2)_x(\text{CH}_3\text{NH}_3\text{PbI}_3)_{1-x}$ where the changes of band gap are visible. (d) The UV-vis spectra of FTO glass/ TiO_2 films filled with $(5\text{-AVA})_x\text{MA}_{1-x}\text{PbI}_3$ and MAPbI_3 . Some images were taken from [49] and [54] with permission.

3.2.2. Doping at site B

The ideal element which suits the organic–inorganic hybrid perovskite structure at site B is Pb, and one can easily refer to the same group elements, for example, Ge or Sn. Javier Navas and his coworkers tried to dope/replace Pb^{2+} with Sn^{2+} , Sr^{2+} , Cd^{2+} , and Ca^{2+} and revealed the development of the properties of crystalline phase, band structure (**Figure 9a**), and emission and optical characteristics. Non-covalent interaction (NCI) analysis complemented with the results from electron localization functions (ELFs) indicated that the strength of the dopant-I interaction follows the order with $\text{Cd-I} > \text{Sn-I} \approx \text{Pb-I} > \text{Sr-I}$ for the tetragonal structure [55]. The system of $\text{MASn}_{1-x}\text{Pb}_x\text{I}_3$ was explored in detail at different ratios of Sn and Pb (**Figure 9b**) [18, 56], and optimized hybrid devices were fabricated afterward [57, 58]. In the end, it is worth pointing out that Pb is rather toxic, and environmental friendly materials are urgently needed to replace lead at site B. As far as explored, no other stable element has been found which can fully replace Pb without downgrading the hybrid perovskite devices' performance. Consequently, doping at site B seems to be the dominant approach to resolve the above-mentioned challenges.

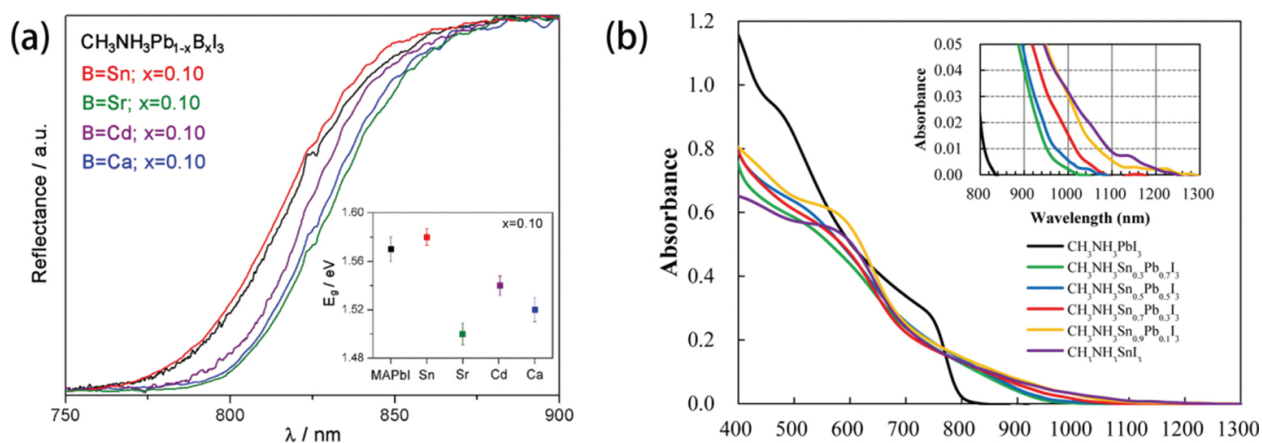


Figure 9. (a) Diffuse reflectance UV–vis spectra for the MAPbI_3 sample and $\text{MAPb}_{1-x}\text{B}_x\text{I}_3$, with $\text{B} = \text{Sn}^{2+}$, Sr^{2+} , Cd^{2+} , Ca^{2+} , and $x = 0.10$. In the inset, the plot of the optical band gap values for each sample. (b) Electronic absorption spectra of perovskite $\text{CH}_3\text{NH}_3\text{Sn}_x\text{Pb}_{(1-x)}\text{I}_3$ coated on porous TiO_2 . Images were taken from [55] and [56] with permission.

3.2.3. Doping at site X

Site X, usually occupied by halogen atoms, typically was iodine at beginning and was attempted with doping of Cl afterward which encouragingly claimed the improvement of both diffusion length and carrier lifetime [14, 58]. Doped $\text{MAPbI}_{3-x}\text{Cl}_x$ has highly oriented crystalline structures exemplified through the strong (1 1 0), (2 2 0), and (3 1 0) peaks attributed to the tetragonal phase [59, 60]. As discovered previously, the variation of the film crystalline orientation order does not impose effect on the photovoltaic performance of the hybrid perovskite devices. [61]. The influence of doping of Cl is not only on the crystalline structure but also on its formation route of perovskite structure. As reported, doping a little amount of Cl in MAPbI_3 perovskite film serves as the nucleation sites to form suitable surface coverage

of perovskite film [62]. Moreover, $\text{MAPbI}_{3-x}\text{Cl}_x$ -based hybrid solar cell changes both the phase and optical properties by optimizing the annealing temperature [63], as also discovered by our group recently with an *in situ* investigation of the improvement of structure and performance of $\text{MAPbI}_{3-x}\text{Cl}_x$ perovskite device by annealing [64], as present in **Figure 10a** and **b**. In most instances, optimized annealing temperature will enhance the PCE in the Cl-doped system, although the PCE may also be reduced after proper annealing in a few cases [65], since the performance of perovskite solar cell depends strongly on the preparation of film formation and crystallization [66, 67]. Interestingly, planar structure comprising $\text{CH}_3\text{NH}_3\text{PbI}_{3-x}\text{Cl}_x$ film exhibits the p-doping character and therefore, a p-n heterojunction was formed when contacted with the n-doped TiO_2 compact layers [68]. The formation energy of mixed halide perovskite was determined by annealing temperature as also verified by theoretical calculations [69].

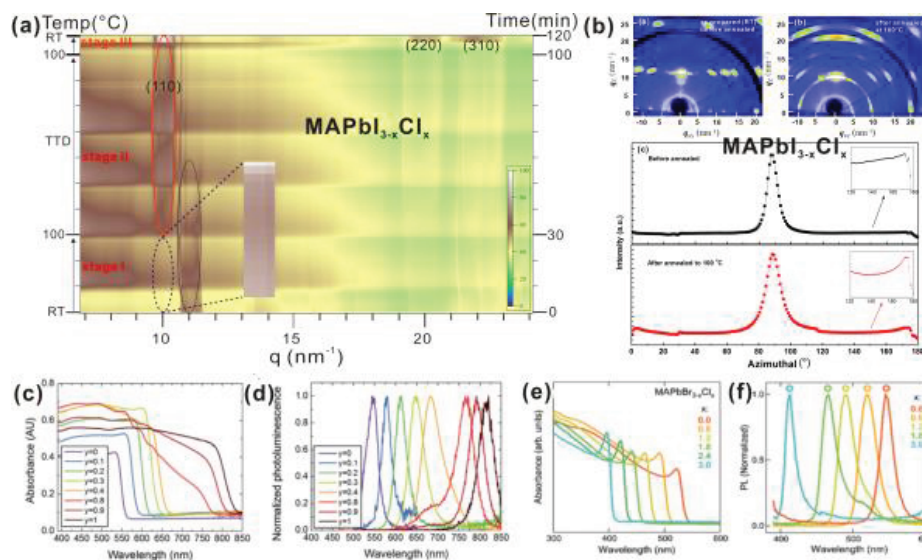


Figure 10. (a) The tunability of band gap and structure in the mixed halide perovskite system. (b) The perovskite structure transformation for the Cl-doped MAPbI_3 film during programmed annealing investigated with conventional and two dimensional XRD. (c) UV-vis of the $\text{FAPbI}_y\text{Br}_{3-y}$ perovskites with varying y . (d) The related photoluminescence spectra for the same films. (e) and (f) Optical absorbance and photoluminescence spectra (370 nm excitation) of $\text{MAPbBr}_{3-x}\text{Cl}_x$ films. Figure (c, d, e, f) were taken from [47] and [73] with permission.

Apart from the doping of Cl, Br has also been tried to partly replace I at the site X. In fact, bromide has been effectively used to tune the band gap of perovskite films. UV and PL spectrum are shown for various doping of Br from 0 to 100% in $\text{CH}_3\text{NH}_3\text{PbI}_3$ perovskite films in **Figure 10c** and **d** [47]. For the synthesis the perovskite $\text{CH}_3\text{NH}_3\text{PbI}_{3-x}\text{Br}_x$ doping the MAI and PbI_2 solution with MABr can change the band gap, which overlaps the whole usable solar spectrum for perovskite solar cells and shifts the XRD peak due to the different ratio of MABr and MAI [70]. The calculation for mixed halide has also been done using first principle calculations. For example, Herz et al. studied the charge carrier dynamics and mobility in formamidinium lead-mixed-halide perovskites and found that the auger recombination constant exists in the mixed halide perovskite system which strongly depends on the value of y in $\text{FAPb}(\text{Br}_y\text{I}_{1-y})_3$ [71]. Besides, lowering the energetic disorder in mixed-halide perovskites

would significantly improve charge carrier transport, allowing effective incorporation in planar-heterojunction tandem solar cells with high short-circuit currents, open-circuit voltages, and PCEs [71]. Perovskite solar cell based on $\text{CH}_3\text{NH}_3\text{SnI}_{3-x}\text{Br}_x$ has been fabricated as a lead-free hybrid device with PCE getting to 5.73% [72]. The last combination of doping with halides can be Cl and Br. $\text{CH}_3\text{NH}_3\text{Pb}(\text{Br}_x\text{Cl}_{1-x})_3$ was used as different types of light emitting diodes (LEDs) due to different energy gaps induced from different doping ($0 < x < 1$) [73, 74]. Such $\text{CH}_3\text{NH}_3\text{Pb}(\text{Br}_{1-x}\text{Cl}_x)_3$ -based hybrid devices with different inclusion of Cl exhibit different electronic structures and the band gap gets broadened after the inclusion of Cl [75]. The optical properties are shown, respectively, in **Figure 10e** and **f**.

Another choice of doping at the site X could be the utilization of anion. $\text{MAPbI}_{3-x}(\text{BF}_4)_x$ has a band gap of 1.5 eV slightly lower than that of MAPbI_3 , and the absorption wavelength is around 827 nm, where the sunlight spectrum has stronger irradiance compared to the absorption wavelength of 800 nm for MAPbI_3 . $\text{MAPbI}_{3-x}(\text{BF}_4)_x$ was proved to own good properties such as good electrical conductivity and high photo response [76]. $\text{MAPb}(\text{SCN})_2\text{I}$ was demonstrated to show high stability in moisture environment compared to MAPbI_3 , and the fabrication process is rather similar [77].

3.2.4. Mixed doping

The MAPbI_3 -PEOXA precursor was used as the sensitizer of hybrid perovskite solar cell to improve the interface morphology of the perovskite-polymer films and to reduce the undesired contact between PEDOT:PSS and PCBM layers for the minimized shunting path at the device [78]. It can be concluded now that the main point for doping hybrid perovskite device is that the proper parameters of t , μ , nice morphology, and robust structure to moisture as well as high performance should be ensured when faced with various choices of doping.

3.3. HTL doping

3.3.1. NiO_x

NiO (as shown in **Figure 11a**) is a relatively rare material which has a nature of p-type semiconductor in both perovskite device and dye-sensitized solar cells, so it is a promising candidate for hybrid devices. The NiO_x thin film is very compact without pinholes which can block the electrons very effectively [79]. Therefore, it is expected that NiO_x doping can improve the properties of hybrid organic inorganic devices. For example, Cu-doped NiO_x increases the electron transmission significantly and enhances the PCE from 8.9 to 15.4% in the inverted structured solar cell [80]. Afterward, low-temperature process for the doping of Cu has been reported [81]. Ni_xMg_{1-x}O was also used as HTL and led to large-area and stable devices with higher PCE [82]. Therefore, we can say that the NiO_x will replace the organic HTL due to its commercial future.

Moreover, graphene oxide (GO) was proved to be a promising candidate as HTL, owing to the enhanced crystallization, high surface coverage ratio, and preferred in-plane orientation of the (110) plane of perovskite film on top. Efficient hole extraction and the enhanced stability of

hybrid devices were demonstrated in the GO-based inverted devices, as reported by our group [83] and other studies [84]. CuI is another inorganic material used as HTL which is a p-type semiconductor and has a matched band structure with the perovskite films [85].

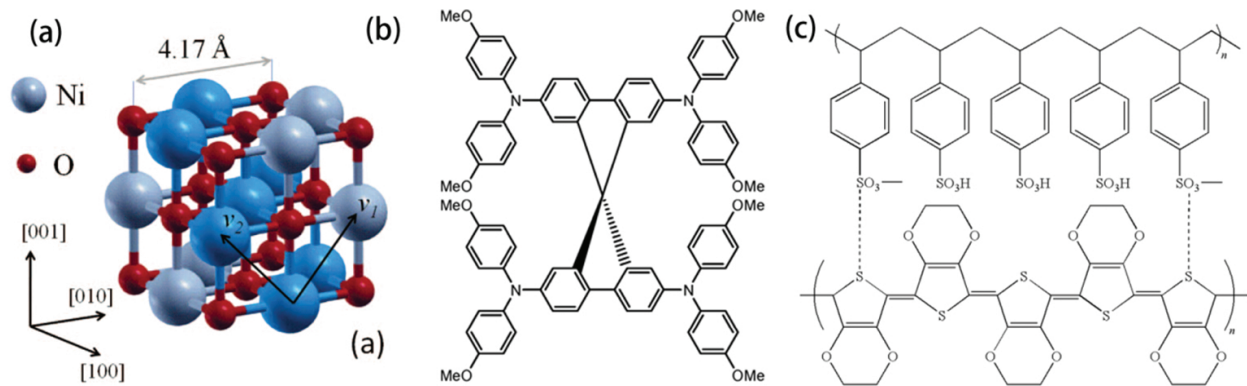


Figure 11. (a) Structure of NiO; (b) structure of spiro-OMeTAD; (c) structure of PEDOT:PSS.

3.3.2. Spiro-MeOTAD and PEDOT:PSS

Spiro-MeOTAD (shown in **Figure 11b**) was also used as HTL as an alternate which supports great PCE for the fabricated devices [86, 87]. However, all of the Spiro-MeOTAD based layers need to be doped because of the nature of such material with bad charge transmission. For instance, Spiro-OMeTAD doped with iodide-reduced graphene oxide has increased the stability of corresponding device and reduced the cost of fabrication. Spiro-MeOTAD116 was doped with Co(III) complex as a p-type dopant for the HTL to ensure a sufficient conductivity and low series resistance [88, 89]. The n-type doped Spiro-OMeTAD functionalized as the pinhole-free HTL has a proper band structure which matches well the band of perovskite film [90].

Moreover, dopant-free PBDTTT-C polymer [91], dopant-free spiro-CPDT [92], dopant-free TPB [93], and dopant-free linear acene derivative were also utilized as the hole transport material [94]. These materials are used as HTL for their appealing properties to replace Spiro-OMeTAD.

PEDOT:PSS (shown in **Figure 11c**) is always designed as the HTL in inverted hybrid perovskite devices, but its acidic characteristics severely threaten long-term stability and performance [95]. Thus, the substitute was explored and found and, for example, CPE-K which contributes to a better performance of the related device [96], is gradually used as HTL. In fact, graphene can not only be used in ETL but also in HTL. PEDOT:PSS doped with graphene quantum rings (GQRs) ensures the efficient hole extraction in hybrid solar cells and relatively high PCE. Hydrophilic graphene oxide doping in PEDOT:PSS composited films demonstrated a PCE of 1.8 times higher than that of the hybrid electronics based on the pristine PEDOT:PSS buffer layer [97]. Besides, PTAA (Poly[bis(4-phenyl)(2,5,6-trimethylphenyl)amine], P3HT (poly(3-hexylthiophene)), PCPDTBT (Poly[2,6-(4,4-bis-(2-ethylhexyl)-4H-cyclopenta[2,1-b;3,4-b']dithiophene)-alt-4,7(2,1,3-benzothiadiazole)]), VB-DAAF (vinylbenzyl 9,9-

diarylfluorene-based triaryldiamine), etc. are also used as HTL for their cheap cost, easy synthesis, and better performance. Actually, the fabricated devices showed higher PCE and better performance than the commonly used PEDOT:PPS and Spiro-MeOTAD materials [98–101].

4. Conclusion

In conclusion, the physical structure and electronic and optical properties of hybrid organic–inorganic perovskite electronics have been illustrated in detail, which sheds new light on the implication of solar cell industry. Driven by the urgent concerns from hybrid perovskite device, doping into the perovskite solar cell is explored by researchers in order to get stable devices with high performance. The progress of *in situ* doping of perovskite electronics from worldwide has been reviewed in this chapter, including the achievement from our group. The doping of ETL promotes the electron transmission, enhances the surface smoothness, blocks holes effectively, reduces the traps, and promotes the PCE for the device ultimately. Second, the doping of perovskite film itself is discussed regarding the doping at sites A, B, and X. Doping at site A leads to a higher PCE, which is associated with better absorption of sunlight according to the UV spectrum. Doping at site B mainly contributes to the environment friendliness with the final goal to get lead-free hybrid devices. Doping at site X can easily tune the band gap of perovskite films to absorb more sunlight with different wavelengths, making the interface more suitable for the electron transmission. Organic HTL (Spiro-MeOTAD) is expensive and needs to be doped to become a p-type semiconductor, so new kind of Spiro-MeOTAD-like materials are synthesized at low cost without doping to improve the hole blocking and electron transmission. Another organic HTL–PEDOT:PPS is also discussed due to its wide usage and easy fabrication by solution process. In all, the PCE of the hybrid perovskite solar cell increases rapidly one study by one study, while the doping promotes the performance of such hybrid organic–inorganic electronics, which is expected to be the third generation of solar cell in the near future.

Author details

Kongchao Shen^{1,2*}, Hao Liang Sun¹, Gengwu Ji¹, Yingguo Yang¹, Zheng Jiang¹ and Fei Song¹

*Address all correspondence to: songfei@sinap.ac.cn

1 Shanghai Institute of Applied Physics, Chinese Academy of Sciences, Shanghai, P. R. China

2 Department of Physics, Zhejiang University, Hangzhou, P. R. China

References

- [1] Kojima, A., et al. Organometal halide perovskites as visible-light sensitizers for photovoltaic cells. *J Am Chem Soc.* 2009; 131:6050.
- [2] Bi, D., et al. Efficient luminescent solar cells based on tailored mixed-cation perovskite. *Sci Adv.* 2016; 2: e1501170.
- [3] Sum, T. C., et al. Advancements in perovskite solar cells: photophysics behind the photovoltaics. *Energy Environ Sci.* 2014; 7: 2518.
- [4] Ponseca, C. S., et al. Organometal halide perovskite solar cell materials rationalized: ultrafast charge generation, high and microsecond-long balanced mobilities, and slow recombination. *J Am Chem Soc.* 2014; 136: 5189.
- [5] Li, C., et al. Formability of ABX₃ (X= F, Cl, Br, I) halide perovskites. *Acta Crystallogr B.* 2008; 64: 702.
- [6] Kim, H.-S., et al. Organolead halide perovskite: new horizons in solar cell research. *J Phys Chem C.* 2014; 118: 5615–5625.
- [7] Green, M. A., et al. The emergence of perovskite solar cells. *Nat Photon.* 2014; 8: 506.
- [8] Chen, Q., et al., Under the spotlight: the organic–inorganic hybrid halide perovskite for optoelectronic applications. *Nano Today.* 2015; 10: 355.
- [9] Liu, Y., et al., Two-inch-sized perovskite CH₃NH₃PbX₃ (X = Cl, Br, I) crystals: growth and characterization. *Adv Mater.* 2015; 27: 5176.
- [10] Huang, J., et al. Organometal trihalide perovskite single crystals: a next wave of materials for 25% efficiency photovoltaics and applications beyond? *J Phys Chem Lett.* 2015; 6: 3218.
- [11] Saidaminov, M. I., et al. High-quality bulk hybrid perovskite single crystals within minutes by inverse temperature crystallization. *Nat Commun.* 2015; 6: 7586.
- [12] Eperon, G. E., et al. Morphological control for high performance, solution-processed planar heterojunction perovskite solar cells. *Adv Funct Mater.* 2014; 24: 151.
- [13] Etgar, L., et al., Mesoscopic CH₃NH₃PbI₃/TiO₂ heterojunction solar cells. *J Am Chem Soc.* 2012; 134: 17396.
- [14] Stranks, S. D., et al., Electron–hole diffusion lengths exceeding 1 micrometer in an organometal trihalide perovskite absorber. *Science.* 2013; 342: 341.
- [15] Ball, J. M., et al. Low-temperature processed meso-superstructured to thin-film perovskite solar cells. *Energy Environ Sci.* 2013; 6: 1739.
- [16] Dong, Q. F., et al. Electron–hole diffusion lengths > 175 μm in solution-grown CH₃NH₃PbI₃ single crystals. *Science.* 2015; 347: 967–970.

- [17] Chueh, C., et al. Recent progress and perspective in solution-processed interfacial materials for efficient and stable polymer and organometal perovskite solar cells. *Energy Environ Sci.* 2015; 8: 1160.
- [18] Stoumpos, C. C., et al. Semiconducting tin and lead iodide perovskites with organic cations: phase transitions, high mobilities, and near-infrared photoluminescent properties. *Inorg Chem.* 2013; 52: 9019.
- [19] Zhang, W., et al. Ultrasoft organic–inorganic perovskite thin-film formation and crystallization for efficient planar heterojunction solar cells. *Nat Commun.* 2015; 6: 6142.
- [20] Yang, B., et al. Perovskite solar cells with near 100% internal quantum efficiency based on large single crystalline grains and vertical bulk heterojunctions. *J Am Chem Soc.* 2015; 137: 9210.
- [21] Sung, S. D., et al. 50 nm sized spherical TiO₂ nanocrystals for highly efficient mesoscopic perovskite solar cells. *Nanoscale.* 2015; 7: 8898.
- [22] Manseki, K., et al. Mg-doped TiO₂ nanorods improving open-circuit voltages of ammonium lead halide perovskite solar cells. *RSC Adv.* 2014; 4: 9652.
- [23] Zhou, H., et al. Interface engineering of highly efficient perovskite solar cells. *Science.* 2014; 345: 542.
- [24] Nagaoka, H., et al. Zr Incorporation into TiO₂ electrodes reduces hysteresis and improves performance in hybrid perovskite solar cells while increasing carrier lifetimes. *J Phys Chem Lett.* 2015; 6: 669.
- [25] Yin, X., et al. Performance enhancement of perovskite-sensitized mesoscopic solar cells using Nb-doped TiO₂ compact layer. *Nano Res.* 2015; 8: 1997.
- [26] Wang, J. T., et al. Low temperature processed electron collection layers of graphene / TiO₂ nanocomposites in thin film perovskite solar cells. *Nano Lett.* 2014; 14: 724.
- [27] Zhu, Z., et al. Efficiency enhancement of perovskite solar cells through fast electron extraction: the role of graphene quantum dots. *J Am Chem Soc.* 2014; 136: 3760.
- [28] Roose, B., et al. Doping of TiO₂ for sensitized solar cells. *Chem Soc Rev.* 2015; 44: 8326.
- [29] Han, G. S., et al. Reduced graphene oxide/mesoporous TiO₂-nanocomposite based perovskite solar cells. *ACS Appl Mater Interface.* 2015; 7: 23521.
- [30] Abrusci, A., et al. High-performance perovskite-polymer hybrid solar cells via electronic coupling with fullerene monolayers. *Nano Lett.* 2013; 13: 3124.
- [31] Zhang, J., et al. Fast and low temperature growth of electron transport layers for efficient perovskite solar cells. *J Mater Chem A.* 2015; 3: 4909.
- [32] Mahmood, K., et al. Double-layered ZnO nanostructures for efficient perovskite solar cells. *Nanoscale.* 2014; 6: 14674.

- [33] Magne, C., et al. Effects of ZnO film growth route and nanostructure on electron transport and recombination in dye-sensitized solar cells. *J Mater Chem A*. 2013; 1: 2079.
- [34] Law, M., et al. Nanowire dye-sensitized solar cells. *Nat Mater*. 2005; 4: 455.
- [35] Mahmood, K., et al. Double-layered ZnO nanostructures for efficient perovskite solar cells. *Nanoscale*. 2014; 6: 14674.
- [36] Cheng, Y., et al. Decomposition of organometal halide perovskite films on zinc oxide nanoparticles. *ACS Appl Mater Interface*. 2015; 7: 19986.
- [37] Zhang, H., et al. Photocorrosion inhibition and photoactivity enhancement for zinc oxide via hybridization with monolayer polyaniline. *J Phys Chem C*. 2009; 113: 4605.
- [38] Peng, G., Xu, X. & Xu, G. Hybrid organic–inorganic perovskites open a new era for low-cost, high efficiency solar cells. *J Nanomater*. 2015; 1: 241853.
- [39] Kim, S. S., et al. Performance enhancement of planar heterojunction perovskite solar cells by n-doping of the electron transporting layer. *Chem Commun*. 2015; 51: 17413.
- [40] Xia, F., et al., Efficiency enhancement of inverted structure perovskite solar cells via oleamide doping of PCBM electron transport layer. *ACS Appl Mater Interface*. 2015; 7: 13659.
- [41] Kuang, C., et al., Highly efficient electron transport obtained by doping PCBM with graphdiyne in planar-heterojunction perovskite solar cells. *Nano Lett*. 2015; 15: 2756.
- [42] Shao, Y., Xiao, Z., Bi, C., Yuan, Y. & Huang, J. Origin and elimination of photocurrent hysteresis by fullerene passivation in $\text{CH}_3\text{NH}_3\text{PbI}_3$ planar heterojunction solar cells. *Nat Commun*. 2014; 5: 5784.
- [43] Xu, J., et al. Perovskite–fullerene hybrid materials suppress hysteresis in planar diodes. *Nat Commun*. 2015; 6: 7081.
- [44] Zhu, Z., et al. A PCBM electron transport layer containing small amounts of dual polymer additives that enables enhanced perovskite solar cell performance. *Adv Sci*. 2015; DOI: 10.1002/advs.201500353.
- [45] Borriello, I., Cantele, G. & Ninno, D., Ab initio investigation of hybrid organic–inorganic perovskites based on tin halides. *Phys Rev B*. 2008; 77: 235214.
- [46] Pang, S., et al. $\text{NH}_2\text{CH}=\text{NH}_2\text{PbI}_3$: an alternative organolead iodide perovskite sensitizer for mesoscopic solar cells. *Chem Mater*. 2014; 26: 1485.
- [47] Eperon, G. E., et al. Formamidinium lead trihalide: a broadly tunable perovskite for efficient planar heterojunction solar cells. *Energy Environ Sci*. 2014; 7: 982.
- [48] Aharon, S., et al. Temperature dependence of hole conductor free formamidinium lead iodide perovskite based solar cells. *J Mater Chem A*. 2015; 3: 9171.

- [49] Pellet, N., et al. Mixed-organic-cation perovskite photovoltaics for enhanced solar-light harvesting. *Ang Chem Inter Ed.* 2014; 53: 3151.
- [50] Lee, J., Seol, D., Cho, A. & Park, N., High-efficiency perovskite solar cells based on the black polymorph of $\text{HC}(\text{NH}_2)_2\text{PbI}_3$. *Adv Mater.* 2014; 26: 4991.
- [51] Li, H., et al. Performance improvement of $\text{CH}_3\text{NH}_3\text{PbI}_3$ perovskite solar cell by CH_3SH doping. *Nanomater Nanotechnol.* 2016; 6: 24.
- [52] Choi, H., et al. Cesium-doped methylammonium lead iodide perovskite light absorber for hybrid solar cells. *Nano Energy.* 2014; 7: 80.
- [53] Yi, C., et al. Entropic stabilization of mixed A-cation ABX_3 metal halide perovskites for high performance perovskite solar cells. *Energy Environ Sci.* 2016; 9: 656–662.
- [54] Mei, A., et al. A hole-conductor-free, fully printable mesoscopic perovskite solar cell with high stability. *Science.* 2014; 345: 295.
- [55] Navas, J., et al. New insights into organic–inorganic hybrid perovskite $\text{CH}_3\text{NH}_3\text{PbI}_3$ nanoparticles. An experimental and theoretical study of doping in Pb^{2+} sites with Sn^{2+} , Sr^{2+} , Cd^{2+} and Ca^{2+} . *Nanoscale.* 2015; 7: 6216.
- [56] Ogomi, Y., et al. $\text{CH}_3\text{NH}_3\text{Sn}_x\text{Pb}_{(1-x)}\text{I}_3$ Perovskite solar cells covering up to 1060 nm. *J Phys Chem Lett.* 2014; 5: 1004.
- [57] Noel, N. K., et al. Lead-free organic–inorganic tin halide perovskites for photovoltaic applications. *Energy Environ Sci.* 2014; 7: 3061.
- [58] Hao, F., Stoumpos, C. C., Cao, D. H., Chang, R. P. H. & Kanatzidis, M. G. Lead-free solid-state organic–inorganic halide perovskite solar cells. *Nat Photonics.* 2014; 8: 489.
- [59] Niu, G., et al. Review of recent progress in chemical stability of perovskite solar cells. *J Mater Chem A.* 2015; 3: 8970.
- [60] Unger, E. L., et al. Chloride in lead chloride-derived organo-metal halides for perovskite-absorber solar cells. *Chem Mater.* 2014; 26: 7158.
- [61] Guerra, V. L. P., et al. Implications of TiO_2 surface functionalization on polycrystalline mixed halide perovskite films and photovoltaic devices. *J Mater Chem A.* 2015; 3: 20811.
- [62] Tidhar, Y., et al. Crystallization of methyl ammonium lead halide perovskites: implications for photovoltaic applications. *J Am Chem Soc.* 2014; 136: 13249.
- [63] Luo, D., et al. Cubic structure of the mixed halide perovskite $\text{CH}_3\text{NH}_3\text{PbI}_{3-x}\text{Cl}_x$ via thermal annealing. *RSC Adv.* 2015; 5: 85480.
- [64] Yang, Y. G., et al. Annealing induced structural transition and photovoltaic performance of perovskite: an in-situ real-time investigation. (submitted to *ACS Nano*)
- [65] Khatiwada, D., et al. Efficient perovskite solar cells by temperature control in single and mixed halide precursor solutions and films. *J Phys Chem C.* 2015; 119: 25747.

- [66] Docampo, P., et al. Solution deposition-conversion for planar heterojunction mixed halide perovskite solar cells. *Adv Energy Mater.* 2014; 4: 1.
- [67] Barrows, A. T., et al. Efficient planar heterojunction mixed-halide perovskite solar cells deposited via spray-deposition. *Energy Environ Sci.* 2014; 7: 2944.
- [68] Guerrero, A., et al. Electrical field profile and doping in planar lead halide perovskite solar cells. *Appl Phys Lett.* 2014; 105: 133902.
- [69] Yin, W., et al. Anomalous alloy properties in mixed halide perovskites. *J Phys Chem Lett.* 2014; 5: 3625.
- [70] Noh, J. H., et al. Chemical management for colorful, efficient, and stable inorganic-organic hybrid nanostructured solar cells. *Nano Lett.* 2013; 13: 1764.
- [71] Rehman, W., et al. Charge-carrier dynamics and mobilities in formamidinium lead mixed-halide perovskites. *Adv Mater.* 2015; 27: 7938.
- [72] Hao, F., et al. Lead-free solid-state organic-inorganic halide perovskite solar cells. *Nat Photonics.* 2014; 8: 489.
- [73] Comin, R., et al. Structural, optical, and electronic studies of wide-bandgap lead halide perovskites. *J Mater Chem C.* 2015; 3: 8839.
- [74] Sadhanala, A., et al. Blue-green color tunable solution processable organolead chloride-bromide mixed halide perovskites for optoelectronic applications. *Nano Lett.* 2015; 15: 6095.
- [75] Zhang, T., et al. A facile solvothermal growth of single crystal mixed halide perovskite $\text{CH}_3\text{NH}_3\text{Pb}(\text{Br}_{1-x}\text{Cl}_x)_3$. *Chem Commun.* 2015; 51: 7820.
- [76] Nagane, S., et al. $\text{CH}_3\text{NH}_3\text{PbI}_{(3-x)}(\text{BF}_4)_x$: molecular ion substituted hybrid perovskite. *Chem Commun.* 2014; 50: 9741.
- [77] Jiang, Q., et al. Pseudohalide-induced moisture tolerance in perovskite $\text{CH}_3\text{NH}_3\text{Pb}(\text{SCN})_2\text{I}$ thin films. *Angew Chem.* 2015; 54: 11006.
- [78] Xue, Q., et al. Metallohalide perovskite-polymer composite film for hybrid planar heterojunction solar cells. *RSC Adv.* 2015; 5: 775.
- [79] Wang, K., et al. p-type Mesoscopic nickel oxide/organometallic perovskite heterojunction solar cells. *Sci Rep.* 2014; 4: 4756.
- [80] Kim, J. H., et al. High-performance and environmentally stable planar heterojunction perovskite solar cells based on a solution-processed copper-doped nickel oxide hole-transporting layer. *Adv Mater.* 2015; 27: 695.
- [81] Jung, J. W., Chueh, C. & Jen, A. K. Y., A low-temperature, solution-processable, Cu-doped nickel oxide hole-transporting layer via the combustion method for high-performance thin-film perovskite solar cells. *Adv Mater.* 2015; 27: 7874.

- [82] Chen, W., et al. Efficient and stable large-area perovskite solar cells with inorganic charge extraction layers. *Science*. 2015; 350: 944.
- [83] Feng, S. L., et al. High-performance perovskite solar cells engineered by an ammonia modified graphene oxide interfacial layer. *ACS Appl Mater Inter*, in press, DOI: 10.1021/acsami.6b02064.
- [84] Wu, Z., et al. Efficient planar heterojunction perovskite solar cells employing graphene oxide as hole conductor. *Nanoscale*. 2014; 6: 10505.
- [85] Christians, J. A., Fung, R. C. M. & Kamat, P. V., An inorganic hole conductor for organo-lead halide perovskite solar cells. Improved hole conductivity with copper iodide. *J Am Chem Soc*. 2014; 136: 758.
- [86] Ganesan, P., et al. A simple spiro-type hole transporting material for efficient perovskite solar cells. *Energy Environ Sci*. 2015; 8: 1986.
- [87] Li, M., et al. Novel spiro-based hole transporting materials for efficient perovskite solar cells. *Chem Commun*. 2015; 51: 15518.
- [88] Burschka, J., et al. Tris(2-(1H-pyrazol-1-yl)pyridine)cobalt(III) as p-type dopant for organic semiconductors and its application in highly efficient solid-state dye-sensitized solar cells. *J Am Chem Soc*. 2011; 133: 18042.
- [89] Burschka, J., et al. Sequential deposition as a route to high-performance perovskite-sensitized solar cells. *Nature*. 2013; 499: 316.
- [90] Jung, M., Raga, S. R., Ono, L. K. & Qi, Y. Substantial improvement of perovskite solar cells stability by pinhole-free hole transport layer with doping engineering. *Sci Rep*. 2015; 5: 9863.
- [91] Chen, W., et al. Simple planar perovskite solar cells with a dopant-free benzodithiophene conjugated polymer as hole transporting material. *J Mater Chem C*. 2015; 3: 10070.
- [92] Franckevičius, M., et al. A dopant-free spirobi [cyclopenta [2,1-b:3,4-b'] dithiophene] based hole-transport material for efficient perovskite solar cells. *Mate Horiz*. 2015; 2: 613.
- [93] Song, Y., et al. Energy level tuning of TPB-based hole-transporting materials for highly efficient perovskite solar cells. *Chem Commun*. 2014; 50: 15239.
- [94] Kazim, S., et al. A dopant free linear acene derivative as a hole transport material for perovskite pigmented solar cells. *Energy Environ Sci*. 2015; 8: 1816.
- [95] Chen, L., Hong, Z., Li, G. & Yang, Y. Recent progress in polymer solar cells: manipulation of polymer: fullerene morphology and the formation of efficient inverted polymer solar cells. *Adv Mater*. 2009; 21: 1434.

- [96] Choi, H., et al. Conjugated polyelectrolyte hole transport layer for inverted-type perovskite solar cells. *Nat Commun.* 2015; 6: 7348.
- [97] Kim, T., Yang, S. & Park, C. Carbon nanomaterials in organic photovoltaic cells. *Carbon Lett.* 2011; 12: 194.
- [98] Heo, J. H., et al. Efficient inorganic–organic hybrid heterojunction solar cells containing perovskite compound and polymeric hole conductors. *Nat Photon.* 2013; 7: 487.
- [99] Bi, D., Yang, L., Boschloo, G., Hagfeldt, A. & Johansson, E. M. J., Effect of different hole transport materials on recombination in $\text{CH}_3\text{NH}_3\text{PbI}_3$ perovskite-sensitized mesoscopic solar cells. *J Phys Chem Lett.* 2013; 4: 1532.
- [100] Kwon, Y. S., Lim, J., Yun, H., Kim, Y. & Park, T. A diketopyrrolopyrrole-containing hole transporting conjugated polymer for use in efficient stable organic–inorganic hybrid solar cells based on a perovskite. *Energy Environ Sci.* 2014; 7: 1454.
- [101] Chiang, T., et al. Functional p-type, polymerized organic electrode interlayer in $\text{CH}_3\text{NH}_3\text{PbI}_3$ perovskite/fullerene planar heterojunction hybrid solar cells. *ACS Appl Mater Interface.* 2015; 7: 24973.